AIAA JOURNAL
Vol. 48, No. 6, June 2010

# Effect of Pitch Rate on Near-Surface Topology on a Delta Wing

T. Goruney* and D. Rockwell†
*Lehigh University, Bethlehem, Pennsylvania 18015*

DOI: 10.2514/1.J050097

**The near-surface flow structure and topology on a delta wing of moderate sweep angle are investigated using a technique of high-image-density digital particle image velocimetry. The focus is on the time evolution of the surface topology during relaxation of the flow after termination of a pitching maneuver for a wide range of pitch rates. The near-surface patterns at the instant corresponding to termination of the maneuver are a strong function of the magnitude of pitch rate and show substantial differences. On the other hand, irrespective of the severity of the flow distortion at the end of the pitching maneuver, the relaxation of the flow involves the same sequence of universal topological states. Furthermore, it is demonstrated that there exists a critical universal state that marks an abrupt transformation between two distinctly different states of the near-surface topology. Moreover, it is demonstrated that the changes of the topological features observed during the early stages of the relaxation process are analogous to the alterations of the surface patterns obtained for the stationary wing at smaller angles of attack.**

## Nomenclature

| | | |
|---|---|---|
| $BL^+$ | = | positive bifurcation line |
| $BL^-$ | = | negative bifurcation line |
| $C$ | = | chord of planform, mm |
| $F$ | = | focal point |
| $F^+$ | = | focus of attachment |
| $F^-$ | = | focus of separation |
| $N$ | = | nodal point |
| $N^+$ | = | node of attachment |
| $N^-$ | = | node of separation |
| $S$ | = | saddle point |
| $t$ | = | time variable |
| $t_f$ | = | actual time at the end of maneuver, s |
| $t_i$ | = | actual time at the beginning of maneuver, s |
| $t'$ | = | actual time variable |
| $t^*$ | = | dimensionless time variable |
| $t^+$ | = | time variable |
| $U_\infty$ | = | freestream velocity, mm/s |
| $u$ | = | streamwise velocity component |
| $V$, $\underline{V}$ | = | velocity vectors |
| $v$ | = | spanwise velocity component |
| $x$ | = | coordinate in streamwise direction |
| $y$ | = | coordinate in spanwise direction |
| $z$ | = | coordinate in surface normal direction |
| $\alpha$ | = | angle of attack, ° |
| $\alpha_i$ | = | initial angle of attack, ° |
| $\alpha_f$ | = | final angle of attack, ° |
| $\dot{\alpha}C/U_\infty$ | = | dimensionless pitch rate |
| $\Delta\alpha$ | = | maneuvering angle, ° |
| $\Delta t$ | = | maneuvering time, s |
| $\partial$ | = | partial derivative |
| $\Lambda$ | = | sweep angle, ° |
| $\Psi$ | = | streamlines |
| $\langle\cdot\rangle$ | = | time-averaging |
| — | = | mean value |

Received 25 July 2009; revision received 5 February 2010; accepted for publication 20 February 2010. 

*Research Assistant, Department of Mechanical Engineering and Mechanics; tug2@lehigh.edu. Student Member AIAA.

†Paul B. Reinhold Professor, Department of Mechanical Engineering and Mechanics; dor0@lehigh.edu. Member AIAA.

## I. Introduction

THE aerodynamics of unmanned combat air vehicles (UCAVs) and micro air vehicles (MAVs) have been of considerable interest in the past decade. Delta wings undergoing steady flight or unsteady maneuvers generate complex flow patterns, the physics of which must be clearly identified in order to optimize maneuverability and minimize unsteady loading associated with vibration and fatigue. These features are strongly related to the existence of leading-edge vortices and their breakdown, as well as the three-dimensional separation and stall along the surface of the planform.

Delta wings of low and moderate values of sweep angle, i.e., typically $\Lambda < 65°$, are associated with distinctive types of flow patterns, which have been the subject of recent research with numerous applications of different experimental techniques. Gursul et al. [1,2] provided extensive reviews of the unsteady aerodynamics of delta wings of low and moderate sweep angles.

The vortical flow over delta wings of low and moderate sweep angles has major differences, compared with high-sweep planforms. Ol and Gharib [3] reported that the vortices form much closer to the surface of the wing. Therefore, vortex/boundary-layer interaction becomes important, as shown by Gursul et al. [4] and Taylor et al. [5]. Taylor et al. [5] found that Reynolds number has a major effect on the structure of these vortical flows, which is not observed over highly swept wings. Separated and vortical flows are dominant even at very low angle of attack.

In relatively low-Reynolds-number experiments of Ol and Gharib [3] and Miau et al. [6], well-defined vortices are visible, where Reynolds number varied from 1000 to 30,000. The flow over wings of low and moderate sweep angles differs substantially from those documented over highly swept planforms at high angles of attack and Reynolds number. Recent computational (Gordnier and Visbal [7]) and experimental (Taylor et al. [5] and Yaniktepe and Rockwell [8]) studies have demonstrated that a dual-primary-vortex structure exists over delta wings of low and moderate sweep angles at low angles of attack. This dual-vortex structure can also be observed in dye visualizations performed by Yavuz [9]. As the angle of attack increases, the dual-primary-vortex structure is replaced by a classical single primary vortex.

A great deal of effort has been focused on the study of the flow structure and topology on stationary delta wings. A wide range of investigations, both experimental and numerical, have addressed the surface topology on planar and nonplanar surfaces, including the simplified planforms of delta wings. Some examples are the studies of Legendre [10], Hunt et al. [11], Tobak and Peake [12], Moffat and Tsinober [13], Peake and Tobak [14,15], Perry and Hornung [16], Perry and Chong [17], Dallman and Schulte-Werning [18], Su et al. [19], Lazos [20], Gordnier and Visbal [7], and Taylor and Gursul [21].

Su et al. [19] classified the types of separated flows above stationary delta wings in relation to the topology along the surface of the wings for a wide range of sweep angle $\Lambda$ and angle of attack $\alpha$ by traditional oil-film flow visualization technique. They report nine different types of separated flow. For low values of $\alpha$, there is a three-dimensional bubble near the leading edge of the wing but the free shear layer does not roll up into a vortex. As $\alpha$ increases, a bubble vortex appears above the wing of small $\Lambda$ where the free shear layer has rolled up but no concentrated vortex core is formed. For large $\Lambda$, two arrays of streamwise vortices appear on each half of the wing. As $\alpha$ increases further, the streamwise vortices on a half wing interact with each other and combine to form a concentrated vortex, but no vortex bursting is evident.

Su et al. [19] define the bursting vortex as a vortex with a bursting point located between the trailing edge and the apex of the wing. Two types of skin-friction line patterns are associated with the bursting vortex: a kink point on the secondary separation line of a wing of large $\Lambda$ and a focal point at the end of the secondary separation line of a wing of small $\Lambda$. For a wing of large $\Lambda$ and sufficiently large $\alpha$, an asymmetric vortex appears. After the bursting point has moved toward the apex, spiral flow patterns occur in the surface flow topology, whereby two foci of separation are located on each half of the wing, and there is unsteady vortex shedding from these points. The reversed flow is characterized by reversal of the flow direction near the upper surface, whereas the completely separated flow is characterized by a node of attachment on the upper surface of the wing.

There has been less emphasis on the unsteady aspects of flow over maneuvering wings, although they are of great importance in terms of aircraft stability and control. Reviews of the unsteady flow structure on delta wings along with the aspects of the vortex breakdown were provided by Rockwell [22] and Visbal [23].

Maltby et al. [24] performed the earliest investigation of unsteady flow phenomena over delta wings involving flow visualization over a delta wing oscillating in heave, as indicated by Gursul [25]. They found the existence of a phase lag of the motion of the vortex core, compared to its variation in the stationary case. Lambourne et al. [26] investigated the behavior of the leading-edge vortices over a delta wing following the termination of pitching maneuver. Gursul [25] emphasized the similarity between the spatial response of the vortex core and to that of a first-order dynamic system to a step function input, and thereby, a phase lag in the variation of the position of the vortex core was expected.

Gad-el-Hak and Ho [27] performed flow visualizations on pitching delta wings, and indicated that the leading-edge vortices exhibited a growth-decay cycle along with the existence of a hysteresis loop in flow patterns for the case of a periodically pitching delta wing. This shows the existence of a time lag in the evolution of the crossflow patterns due to pitching motion. One might also expect the existence of a similar time lag phenomenon for the near-surface flow patterns.

Gursul and Yang [28] carried out unsteady pressure measurements on a pitching delta wing of 70° sweep angle in order to investigate the effects of pressure gradient on the phase lag between the wing motion and the movement of breakdown location. They hypothesized and showed that the phase delay of the breakdown location for pitching delta wings may be related to the variations of the adverse pressure gradient on the wing surface, based on the suggestion of Gursul and Ho [29] that delta-wing vortex breakdown in unsteady flow is driven by the external pressure gradient.

Miau et al. [30] visualized the flow patterns on pitching delta wings via dye visualization and laser Doppler anemometry measurements. Visbal and Gordnier [31] computationally characterized the effect of pitch rate and the location of the pitch axis on the onset of vortex breakdown.

Reynolds and Abtahi [32], Magness et al. [33], and Jarrah [34] provided information about the response of the vortex breakdown during transient maneuvers. Atta and Rockwell [35] and LeMay et al. [36] investigated the response of flow patterns on delta wings to a harmonic pitching maneuver. Woffelt [37] addressed both of these types of pitching motions. Lin and Rockwell [38] defined the region of vortex breakdown in terms of critical points of the sectional topology, as well as patterns of azimuthal vorticity. Visbal and Gordnier [31] provided numerical simulations of these features in a parallel investigation.

Magness et al. [39] characterized the instantaneous crossflow topology of the unsteady leading-edge vortex on a delta wing of 70° sweep angle. They defined a new topological structure for flow over a delta wing undergoing transient pitching maneuvers at high angle of attack. That is, the leading-edge vortex was found to exhibit an outward-spiraling pattern corresponding to an unstable focus.

The near-surface patterns of streamline topology on a pitching wing (38.7° sweep angle) at instants of time following termination of a maneuver were investigated by Yavuz et al. [40]. The corresponding relaxation process including the time evolution of critical features was represented. Yavuz [9] characterized the effect of the pitch rate on crossflow patterns.

The present investigation characterizes the time evolution of the flow structure and near-surface topology on a pitching delta wing of moderate sweep angle for a wide range of pitch rate using critical-point concepts in order to gain an understanding of the flow physics associated with flow along a maneuvering delta wing.

## II. Experimental System and Techniques

An overview of the experimental setup is given in Fig. 1a. The sweep angle of the delta wing had a value of $\Lambda = 50°$. The root chord of the wing was $C = 200$ mm, and the wing thickness was 6.35 mm, with 30° beveling on the windward side. All experiments were performed at a Reynolds number of 15,000.

Experiments were performed in a large-scale water channel. The main test section of this facility had a width of 927 mm and a height of 610 mm; the water level was maintained at 547 mm. Upstream of this test section, a flow conditioning system involving honeycomb and a sequence of five screens provided a turbulence intensity of approximately 0.3%. The freestream velocity in the test section was maintained at 70.9 mm/s. The water flow was seeded with 12-$\mu$m-diam metallic coated plastic spheres, with a sufficient density such that 15–20 particle images were typically attained within the interrogation window. The laser sheet was generated by a dual-pulsed Yag laser system having a maximum output of 50 mJ. The pulse rate of the lasers was 15 Hz. Images during the entire relaxation process were acquired at effective rates of 15 and 5 frames per second. Using a lower framing rate allowed sufficiently long image capture time in order to characterize the flow during the relatively later stages of relaxation.

The schematic of Fig. 1a also shows the location and orientation of the camera employed for digital particle image velocimetry. The sensor array of the camera was $1008 \times 1018$ pixels. To minimize refraction effects and thereby optimize the quality of the particle image patterns, a prism was attached to the exterior of the test section of the water channel, also shown in Fig. 1a. The designated prism was constructed of 3 mm Plexiglas and filled with distilled water.

For the case of the maneuvering wing experiments, a linear ramplike pitching motion was applied between the initial and final angles of attack for a wide range of pitch rate, as illustrated in Fig. 1b. Sequential images were recorded upon completion of the pitching maneuver at an angle of attack of 25° in order to characterize the relaxation process.

The following parameter was defined for the pitch rate during a pitching maneuver:

$$\frac{\dot{\alpha}C}{U_\infty} = \left(\frac{\Delta\alpha}{\Delta t}\right)\left(\frac{C}{U_\infty}\right)$$

where $\Delta\alpha = \alpha_f - \alpha_i$, and $\Delta t$ is the time difference between the initial and final values of angle of attack, defined, respectively, as $\alpha_i = 5°$ and $\alpha_f = 25°$. Actual pitch rates [9] of an unmanned combat air vehicle during a maneuver, $\dot{\alpha}C/U_\infty = 0.1$ and 0.2, were considered when defining parameters of the pitching motion. Four different pitch rates were employed: $\dot{\alpha}C/U_\infty = 0.05$, 0.1, 0.2, and 0.4. The elapsed actual time $t'$ is normalized by $U_\infty/C$ to obtain

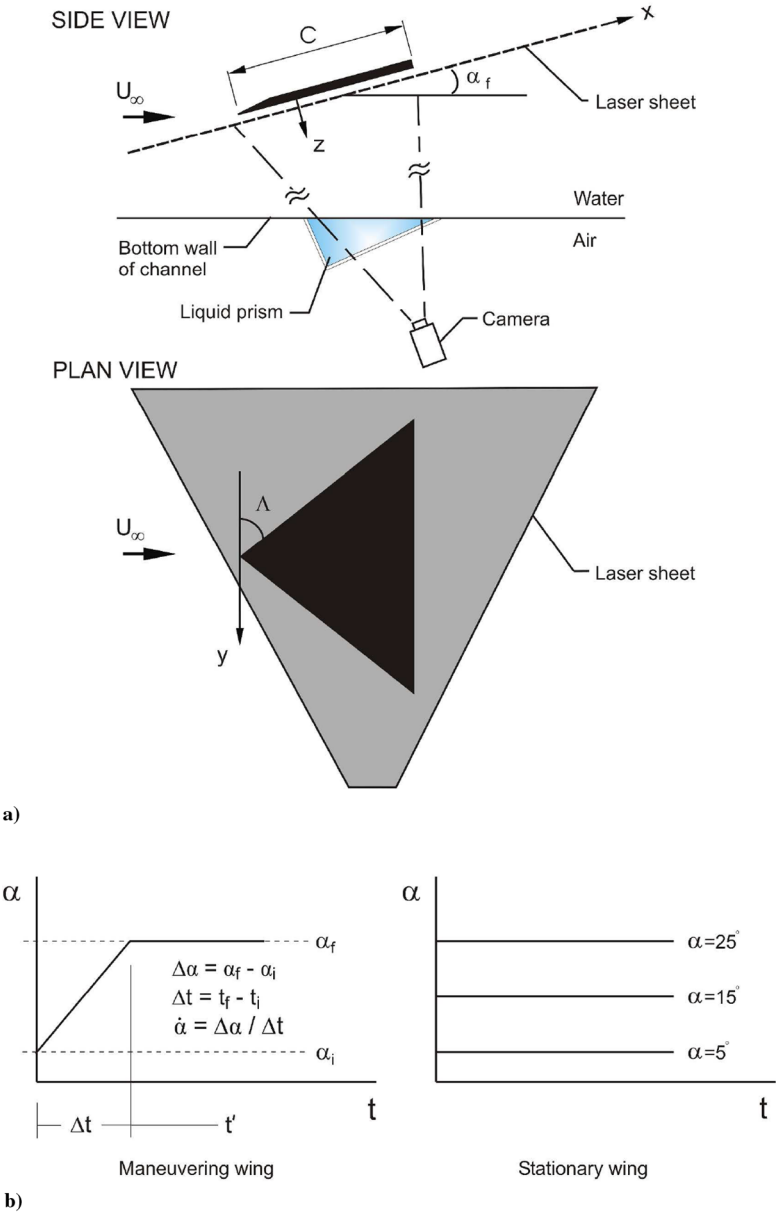


**Fig. 1 Illustrations of a) overview of delta wing and laser sheet orientation for quantitative imaging and b) motion for maneuvering and stationary-wing experiments as a function of time.**

$t^* = t' U_\infty / C$, where $t' = 0$ or $t^* = 0$ corresponds to the termination of the pitching maneuver.

For the stationary-wing experiments, images were recorded at three different values of angle of attack, $\alpha = 5, 15, 25°$. An overview of the stationary-wing experiments is given in Fig. 1b.

Images were acquired at a dimensionless distance from the surface of the wing, i.e., location of the laser sheet, at $z/C = 0.005$. A rigorous assessment of the effects of displacement of the laser sheet in the region close to the wing is provided by Goruney [41]. In essence, in the very near-surface region, changes in elevation of the laser sheet yield only very small changes in the location and form of topological critical points.

Images were evaluated using a frame-to-frame cross-correlation technique with a $32 \times 32$ pixel interrogation window and 50% overlap. The distance from the objective of the camera to the plane of the laser sheet was 1125 mm. Effective values of magnification and the grid size in the physical plane of the laser sheet were 4 pixels/mm and 0.02, respectively. Resolution of the images of the flowfield was optimized by acquiring images over half of the wing. Preliminary experiments, at the outset of this program, verified the symmetric of patterns with respect to the plane of symmetry of the wing. Time-averaged patterns of velocity vectors $\langle \underline{V} \rangle$ were obtained by averaging instantaneous velocity fields $V$ over the entire sequence of approximately 200 images. Other quantitative representations of the flow structure, such as instantaneous and time-averaged streamlines $\Psi$, were deduced from the patterns of velocity vectors.

For the present investigation, the uncertainty in the velocity vectors was in the range of 1.5–2%. The streamlines represent an integral of the velocity field, and the uncertainty of velocity is taken to provide a conservative estimate of the uncertainty of the value of the stream function, which define the streamlines. Regarding position uncertainties, the uncertainty in the distance of the center of the laser sheet relative to the surface of the wing is 0.0005 C.

Regarding qualitative representation of the flow patterns, dye visualization was employed to complement the digital particle image velocimetry technique. The dye visualization images provided herein were shown by Yavuz [9].

## III. Time Evolution of Flow Structure Because of Pitching Motion

Relaxation of the flow patterns after the end of the maneuver are indicated by the dye visualization of Fig. 2. The time sequence of images is designated as $t' = 0$ through 17, where $t'$ corresponds to

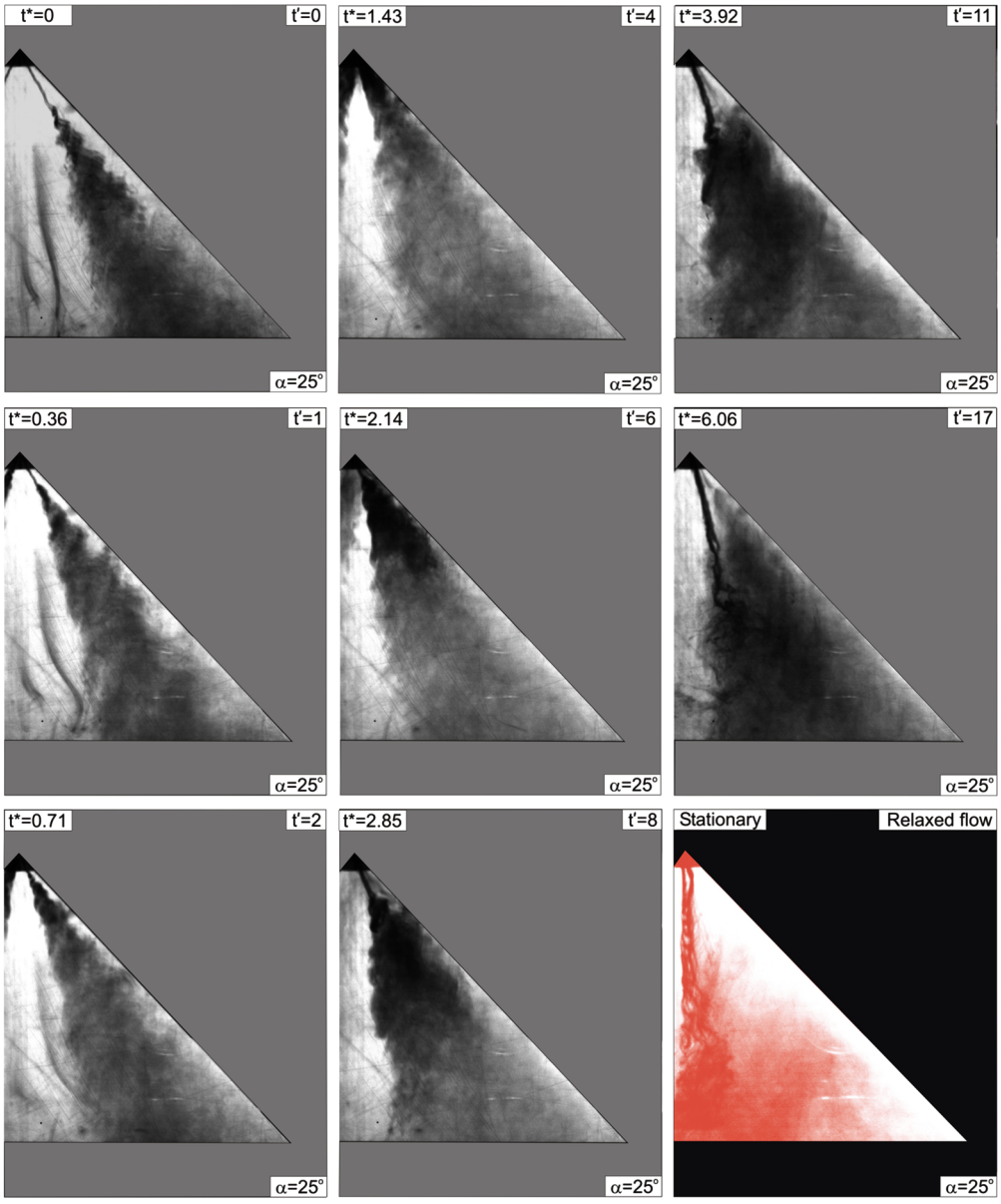


**Fig. 2 Dye visualization of relaxation process after cessation of maneuver, where $t'$ is the actual time in second and $t^* = t'U_\infty/C$ is the dimensionless time after attainment of final angle of attack $\alpha_f$. The pitch-up rate is $\dot{\alpha}C/U_\infty = 0.1$ (from Yavuz [9]).**

the actual time in seconds. The dimensionless time $t^*$ following termination of the pitch-up maneuver is defined as $t^* = t'U_\infty/C$. Values of both $t'$ and $t^*$ are designated on each of the images. The red flow pattern located at the bottom right corner of Fig. 2 corresponds to the stationary wing, which represents the relaxed flow.

The relaxation process shows distinctive types of flow patterns. During the first stage of relaxation, the generic feature is upstream movement of the location of vortex breakdown, which ends with breakdown at the apex of the wing, indicated in the image $t' = 4$. This instant might be called a critical stage of the relaxation process, whereby the leading-edge vortex loses its characteristics. In image $t' = 11$, reverse flow is clearly evident in regions close to the leading edge of the planform. The diluted dye marker near the leading edge does not represent a vortical structure that emanates from the apex; instead, it originates from the dye marker located near the centerline of the planform and extends toward the apex along the leading edge, thereby representative of a reverse flow. At $t' = 17$, relaxation of the flow patterns is nearly achieved, and the flow structure closely resembles that of the stationary case. The dye marker covers nearly the entire planform and clearly indicates the existence of large-scale stall. The vortex filament apparent in images $t' = 8$, 11, and 17 is not associated with the leading-edge vortex and is representative of the attached flow region near the centerline of the planform. It eventually extends along the centerline, as shown in the image corresponding to the stationary-relaxed flow state in Fig. 2. The foregoing observations are consistent with those reported by Yavuz [9], who found that during the relaxation process the well-established single-leading-edge vortex in its breakdown state transforms to a region of three-dimensional separation.

The relaxation process can be defined in terms of sequential states of the quantitative near-surface patterns given in Figs. 3 and 4 for a value of pitch rate $\dot{\alpha}C/U_\infty = 0.2$. The images at $t^* = 0$ in Figs. 3 and 4 correspond to the time at which the pitching motion ends; these, as well as all subsequent images, are therefore acquired at the same angle of attack of 25°. The images at a sufficiently long time $t^* = 13.65$ after termination of the wing motion represent the relaxed state of the flow. The five images at values of $t^*$ extending from $t^* = 0$ and 13.65, shown in Figs. 3 and 4, define the distinct patterns, or states, of the near-surface flow structure during the relaxation process.

Figure 3 shows the near-surface patterns of instantaneous velocity vectors. The flow direction is from left to right. Only half of the wing is shown, due to symmetry. The apex of the delta wing is located in the top left corner in all five images, and the leading edge extends diagonally across each image.

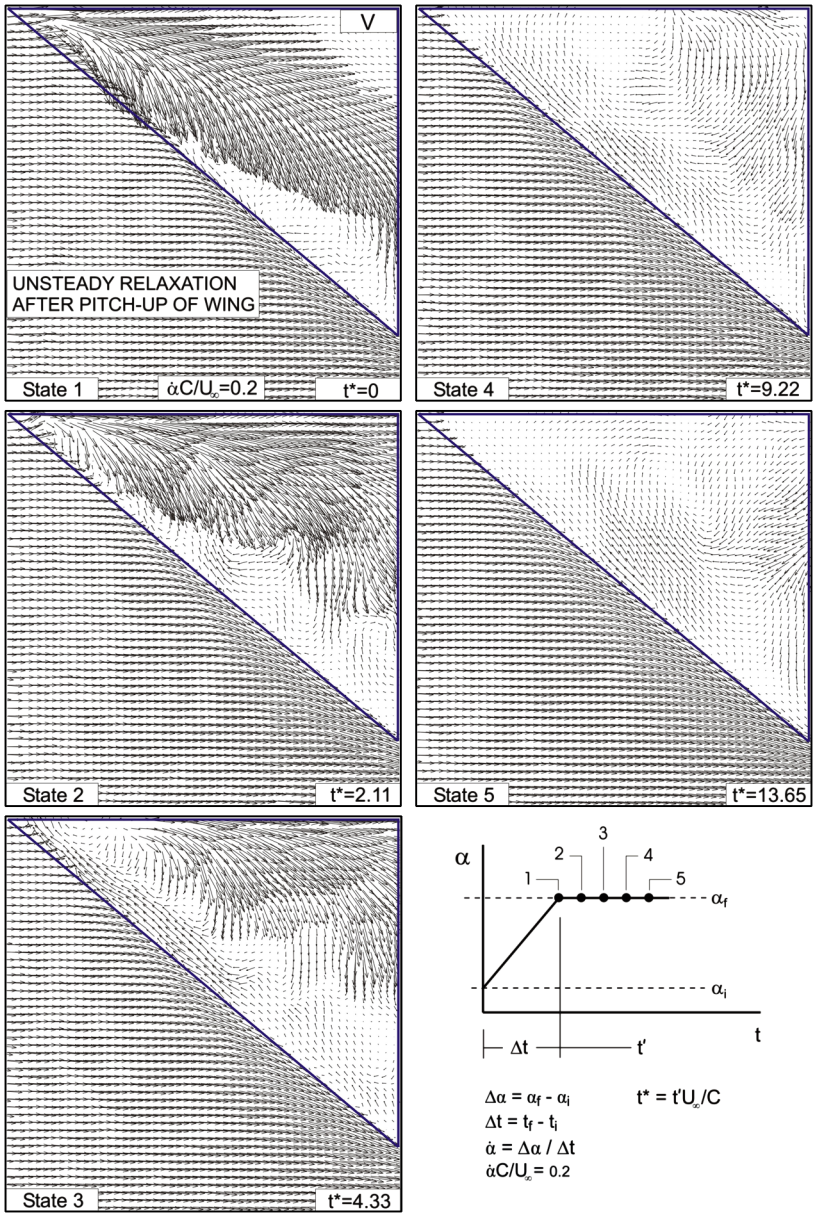


**Fig. 3 Patterns of instantaneous velocity vectors $V$ during the relaxation process after cessation of maneuver as a function of nondimensional time $t^*$. The pitch-up rate is $\dot{\alpha}C/U_\infty = 0.2$.**

Generally speaking, the high magnitudes of the velocity patterns at the termination of maneuver, $t^* = 0$, start to fade out as the flow relaxes, and finally, at the relaxed state, $t^* = 13.65$, the patterns of low velocity magnitude rotate in the clockwise direction, i.e., they form a low magnitude recirculation zone along the wing surface, which indicates the existence of stall.

More specifically, at $t^* = 0$, a jet like flow along the leading-edge vortex is evident and there is no reverse flow on the wing surface. At this instant, the velocity magnitudes along the wing surface are much larger than the magnitudes in the freestream. The leading-edge vortex induces this region of large magnitude along the surface. At $t^* = 2.11$, small-scale recirculation zones start to appear close to the leading edge, while at the location close to the plane of symmetry of the wing, velocity vectors of substantial magnitude are oriented in the streamwise direction.

At $t^* = 4.33$, however, there appears to be a well-defined reverse flow with significant velocity magnitude along the leading edge directed toward the apex of the wing. In addition, close to the apex, a reduction in the magnitude of velocity vectors is evident, relative to the magnitudes that exist in the images at earlier times $t^* = 0$ and 2.11. At $t^* = 9.22$, the magnitude of the reverse flow along the leading edge decreases, and a recirculation pattern becomes evident at about the midchord. Furthermore, the velocity magnitudes have become dramatically smaller over the region of the wing inboard of the leading edge.

The image at $t^* = 13.65$ indicates that the recirculation pattern later forms into a well-defined swirl pattern with extremely low velocity magnitudes, representative of stall.

Considering the entire set of images of Fig. 3, and cross-comparing them with the dye visualization of Fig. 2, it can be stated that the dramatic decrease in the near-surface velocity magnitudes, appearing after $t^* = 2.11$ (in Fig. 3) and $t' = 6$ (in Fig. 2), is an outcome of the leading-edge vortex losing its characteristics when breakdown occurs at the apex of the wing. This observation was originally reported by Yavuz [9], who indicated a critical stage during relaxation following termination of the pitching maneuver. In essence, the reduction of velocity magnitudes along the wing surface is the footprint of the loss of a defined structure of the leading-edge vortex.

Further insight into the flow structure during the relaxation process is provided by patterns of near-surface streamline topology and associated critical points given in Fig. 4, which complement the aforementioned patterns of dye visualization and near-surface velocity vectors.

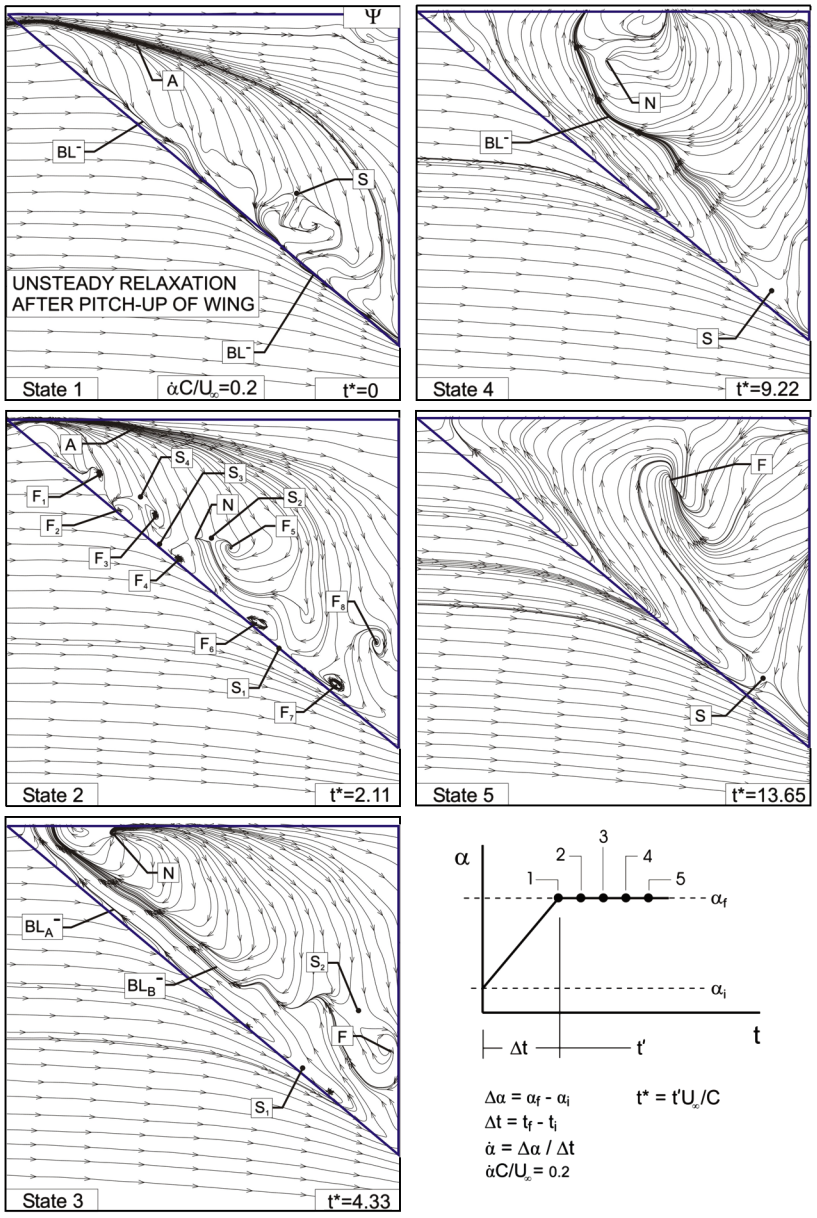


**Fig. 4 Patterns of instantaneous streamline topology Ψ during the relaxation process after cessation of maneuver as a function of nondimensional time $t^*$. The pitch-up rate is $\dot{\alpha}C/U_\infty = 0.2$.**

The image at $t^* = 0$ represents the first state, i.e., state 1 of the near-surface topology. A negative bifurcation line BL⁻ located along the leading edge is oriented in the downstream direction, and there is a positive bifurcation-line-like pattern *A* originating from the apex of the wing. The negative bifurcation line BL⁻ represents two-dimensional separation, whereas the positive bifurcation-line-like *A* indicates reattachment. The footprint of the leading-edge vortex on the wing surface is represented by the orientation of the streamlines from location *A* toward the leading edge.

In state 2, at $t^* = 2.11$, a substantial number of small-scale foci *F*, saddles *S* and nodes *N* appear close to the leading edge, which indicate the presence of small-scale instabilities in the flow. The positive bifurcation-line-like structure *A*, evident at $t^* = 0$, is still detectable. This state 2 of the flow topology at $t^* = 2.11$ is believed to be the most critical one, because it corresponds to transition to the next state, which is substantially different. This critical nature of state 2 is supported by the dye visualization of Yavuz [9]. The small-scale distortions represented by the critical points *F*, *S*, and *N* along the leading edge at $t^* = 2.11$ are associated with loss of identity of the leading-edge vortex, due to the occurrence of breakdown at the apex.

Lamar [42] performed wind-tunnel tests on a half-airplane model of the F-106B at high Reynolds numbers on the order of $10^7$. In addition to the classical leading-edge separation, he reported evidence of other vortical action inboard of the leading edge at an angle of attack of 19° and a Reynolds number of $32 \times 10^6$ on a round-edged cambered delta wing, which was attributed to a flow regime when the leading-edge vortex is not yet strong enough to dominate the entire outer flow. This regime shows resemblance to the aforementioned small-scale instabilities associated with loss of identity of the leading-edge vortex, due to the occurrence of breakdown at the apex.

The wind-tunnel experiments of Riley and Lowson [43] on an 85° swept delta wing at an angle of attack of 12.5° using laser Doppler anemometry revealed a system of streamwise vortical structures, which are associated with low-momentum regions in the separated vortex flow. Similarly, these low-momentum regions show resemblance to the aforementioned small-scale instabilities in that they represent stagnant regions in the flowfield.

State 3 corresponds to the image at $t^* = 4.33$ in Fig. 4. A distinctive feature is a well-defined reverse flow along the leading edge of the wing. Two different negative bifurcation lines, $BL_A^-$ and

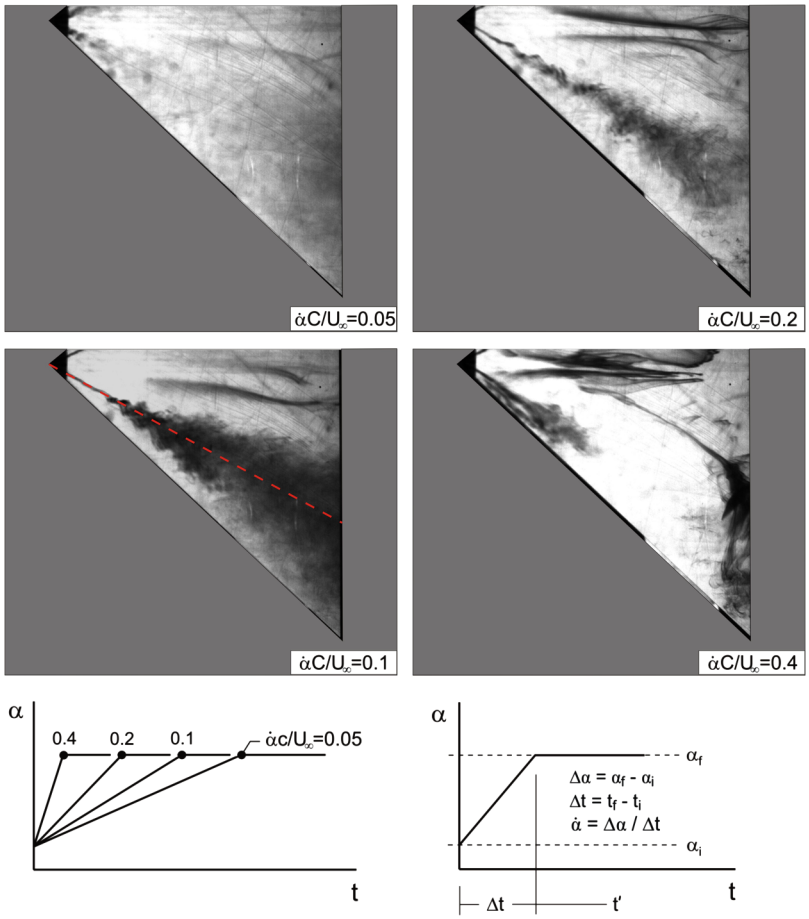


**Fig. 5 Dye patterns at cessation of maneuver for different pitch rates $\dot{\alpha}C/U_\infty$ (from Yavuz [9]). The path of the leading-edge vortex is indicated with red dashed line.**

$BL_B^-$, are visible; they indicate different regions of two-dimensional separation. The positive bifurcation-line-like structure *A* observed in states 1 and 2 at earlier times is replaced by a pattern of streamlines emanating from a single node *N* of attachment.

In state 4 at $t^* = 9.22$, the relatively narrow zone of reverse flow along the leading edge, indicated in the aforementioned state 3, broadens substantially. This process is accompanied by the onset of a large-scale recirculation pattern that appears well inboard of the leading edge. A small-scale node *N* of separation appears within this recirculation pattern. In addition, a saddle point *S* is present close to the intersection of leading and trailing edges.

In state 5, at $t^* = 13.65$, the recirculation pattern shown at $t^* = 9.22$ has evolved into a coherent, large-scale swirl pattern with a well-defined center, i.e., focus *F* of separation, which indicates the occurrence of a three-dimensional separation associated with the onset of stall along the wing surface. The location of the saddle point *S* remains the same as in the previous state 4. In this state 5, the flow has essentially relaxed and its structure closely resembles that of the stationary case.

In the present investigation, the patterns of streamline topology show that both two- and three-dimensional separation are evident from the surface of the delta wing during flow relaxation. At earlier stages of relaxation, the negative bifurcation line near the leading edge of the delta wing represents classical two-dimensional separation in flow over an aerodynamic body under angle of attack. Eventually, once the flow relaxes, the patterns of streamline topology converge to the form that is representative of three-dimensional separation, which is observed in flow over delta wings under sufficiently high angle of attack.

## IV. Effect of Pitch Rate

The effect of pitch rate on the time evolution of the flow structure was demonstrated during the relaxation process following the cessation of pitching motion. Four different pitch rates were investigated.

It turns out that, irrespective of the severity of the flow distortion at the end of the pitching maneuver, the relaxation of the flow involves the same sequence of flow states. It is demonstrated that the time delay to occurrence of the first state is very sensitive to the pitch rate. The delay between subsequent states is, however, nearly independent of pitch rate.

### A. Patterns at Termination of Pitching Maneuver

It is known that a single-leading-edge vortex in its breakdown state will eventually transform to a region of three-dimensional separation. This transformation starts with upstream movement of vortex breakdown toward the apex. Once it reaches the apex, the leading-edge vortex loses its characteristics. A reverse flow close to the leading edge becomes evident, and it later transforms to large-scale separation from the surface. Then the flow relaxes and its structure closely resembles that of the stationary case.

Figure 5 shows dye visualization (Yavuz [9]) at termination of the pitching maneuver for all pitch rates investigated in this study. Because of symmetry, only half of the wing is shown. At termination of the maneuver, i.e., at angle of attack of 25°, the flow starts to relax toward the steady state. Generally speaking, the single-leading-edge vortex is evident, to varying degrees, at all pitch rates.

At the minimum pitch rate, $\dot{\alpha}C/U_\infty = 0.05$, where the severity of the flow distortion is minimal, the vortex is evident only near the apex; the occurrence of large-scale separation generates a diffuse dye pattern. For increasing pitch rate, the onset of large-scale vortex breakdown moves toward the trailing edge. For the case of maximum pitch rate, $\dot{\alpha}C/U_\infty = 0.4$, the leading-edge vortex is in its early stages of formation; the relatively high level of flow distortion causes a discontinuity in the dye pattern.

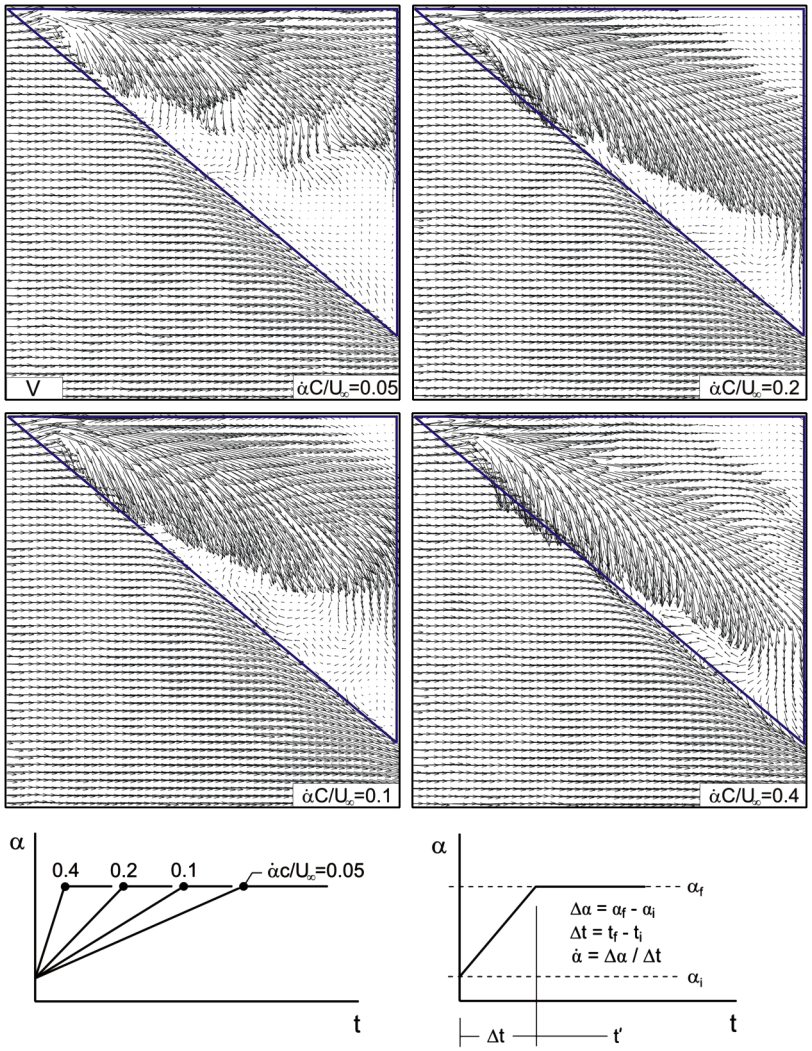


**Fig. 6 Patterns of instantaneous velocity vectors $V$ at cessation of maneuver for different pitch rates $\dot{\alpha}C/U_\infty$.**

Figure 6 shows corresponding patterns of instantaneous velocity vectors at termination of the pitching maneuver for all pitch rates. They are distinctly different. For example, the spatial extent of the region of low magnitude velocity, which is located between the leading edge and the high-magnitude velocity vectors, decreases with increasing pitch rate. A stagnant region is located close to the plane of symmetry at the trailing edge, except for the case of the minimum pitch rate. In essence, a jetlike flow pattern of velocity vectors is evident for all pitch rates. It is deflected toward the leading edge for increasing pitch rate. The aforementioned observations can be correlated with the early onset of vortex breakdown, and loss of identity of the leading-edge vortex, shown in the dye visualization of Fig. 5. This phenomenon can be explained by the fact that the flow patterns at relatively high pitch rates of $\dot{\alpha}C/U_\infty = 0.1$, 0.2, and 0.4, eventually converge to the pattern at $\dot{\alpha}C/U_\infty = 0.05$ at some time during the relaxation process.

Corresponding patterns of instantaneous streamline topology at the termination of the maneuver, which are given in Fig. 7, show several distinctions. The angle between the plane of symmetry of the wing and the pattern of diverging streamlines, designated by the symbol $A$, increases, and the extent of the region enclosed by this streamline pattern and the leading edge decreases as the magnitude of the pitch rate $\dot{\alpha}C/U_\infty$ increases.

Figure 7 shows existence of a bifurcation line $BL^-$ along the leading edge of the wing for all values of pitch rate $\dot{\alpha}C/U_\infty$. The length of this line varies, however, with pitch rate. At $\dot{\alpha}C/U_\infty = 0.05$, it is relatively short and located close to the apex. At higher values of pitch rate $\dot{\alpha}C/U_\infty = 0.2$ and 0.4, it extends along the entire leading edge of the wing. The negative bifurcation line $BL^-$ for relatively small pitch rates $\dot{\alpha}C/U_\infty = 0.05$ and 0.1 can be correlated with the early onset of vortex breakdown. As shown in the top two images of Fig. 7, the large-scale burst region of the vortex interacts with the leading-edge separation region, and causes the bifurcation line $BL^-$ from extending along the entire leading edge.

Figure 7 also shows additional topological features and critical points. The number of critical points decreases with increasing pitch rate. This observation is consistent with the early onset of vortex breakdown at the two lowest values of pitch rate shown in Fig. 5. As the value of $\dot{\alpha}C/U_\infty$ becomes larger, the number of critical points decreases until, at the largest value of $\dot{\alpha}C/U_\infty$, no saddle points $S$ or foci $F$ exist along the leading edge. The highest pitch rate correlates with the dye visualization image at $\dot{\alpha}C/U_\infty = 0.4$ in Fig. 5, which involves formation of the leading-edge vortex following severe flow distortion upon cessation of the maneuver.

### B. Patterns During Relaxation Process

Figures 5–7 show that variations of the pitch rate produce substantially different near-surface flow patterns and topologies, at the instant corresponding to termination of the maneuver. As the flow relaxes from these substantially different initial states, the near-surface topology may pass through a sequence of states, in a manner analogous to the relaxation process shown in Figs. 3 and 4. It may be possible to identify the same states, occurring in an ordered sequence, irrespective of the different initial states produced by different pitch rates. If this can be achieved, it would be possible to define a set of universal states, which would expedite interpretation and analysis of the relaxation process. It is anticipated that such

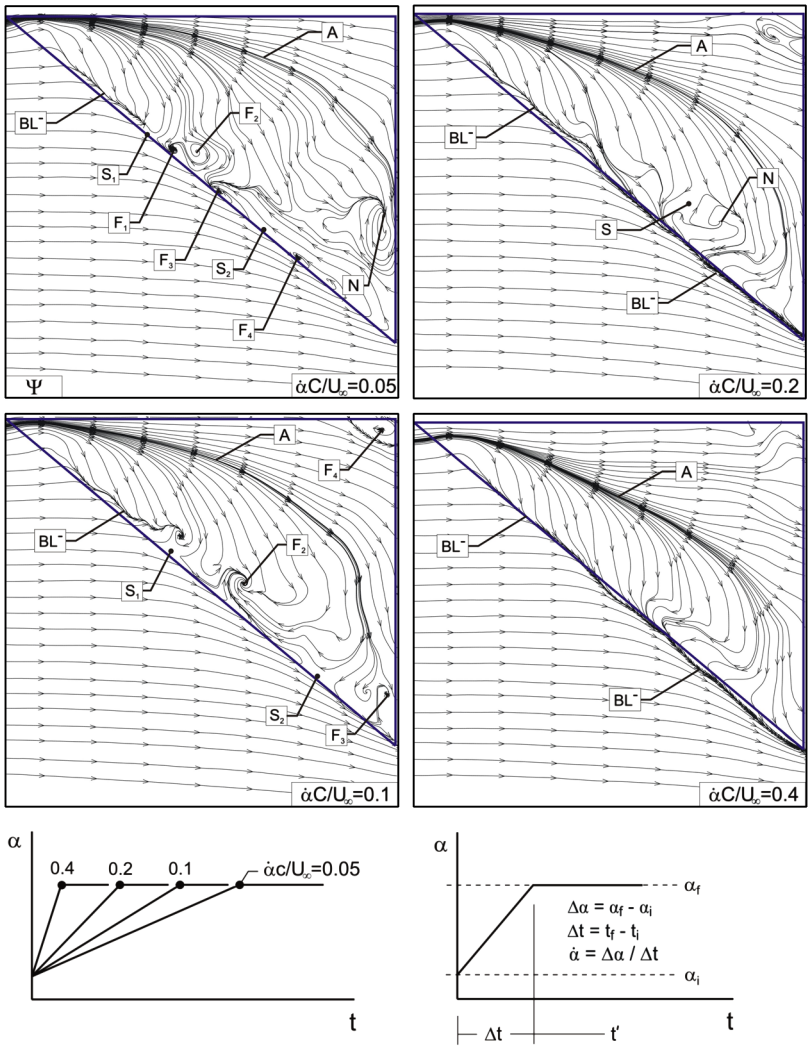


**Fig. 7 Patterns of instantaneous streamline topology Ψ at cessation of maneuver for different pitch rates $\dot{\alpha}C/U_\infty$.**

universal states would occur at different time delays after termination of different pitch-up maneuvers. Such states would therefore provide a basis for analyzing the dimensionless time delays.

Each universal state represents a unique set of critical points and topological patterns where the location of each prominent critical point, such as the node of attachment $N^+$ in state 3 and focus of separation $F^-$ in state 5, remains within 3% of the chord $C$; and the numerical values of expressions $(\partial u/\partial x \cdot \partial v/\partial y - \partial u/\partial y \cdot \partial v/\partial x)$ and $(\partial u/\partial x + \partial v/\partial y)$ evaluated at the corresponding critical points remain within 6% of the chord $C$ in both streamwise and spanwise directions for different pitch rates. These expressions are proportional to the numerical values of Jacobian and divergence, respectively, and therefore determine the type of the critical points.

To illustrate the possibility that the same topological states can occur for different initial conditions, i.e., different states of the flow at the completion of different pitch-up maneuvers, the time sequence of topologies was examined for all of the pitch rates defined in Fig. 7, and each sequence was searched for a state similar to state 3 indicated in Fig. 4. Figure 8 compares the near-surface patterns of instantaneous streamline topology in state 3. The critical points and topological features are indicated. Close to the apex, a node $N$ of attachment is evident in all cases, whereby streamlines emanate from the nodal location $N$. For all cases, two negative bifurcation lines $BL_A^-$ and $BL_B^-$ located along the leading edge are distinguished by the subscripts $A$ and $B$, which indicate two-dimensional separation zones. Again, a saddle $S$ is evident for all pitch rates in the vicinity of the intersection of the leading edge and the trailing edge. The process described in the foregoing was followed for identification of the states 1, 2, 4, and 5, defined in Fig. 4, and they were compared in a similar fashion as for Fig. 8. Because of space limitations, these comparisons are not included herein. It was found that the types and locations of the critical points were very similar for each of the states 1, 2, 4, and 5, irrespective of the value of pitch rate; in other words, the patterns of near-surface topology in a given state are independent of the degree of flow distortion at the end of the maneuver. Henceforth, these very similar states are referred to as universal states.

## V. Universal States Based on Critical Points and Their Time Delay During Relaxation

### A. Definition of Universal States

Figure 9 shows the principal topological features and critical points of the near-surface patterns for the five different universal states described in the previous section. Their physical interpretation is the same as for the sequence of images given in Fig. 4. These five universal states define the essential features of the time evolution of the flow structure on a sharp-edged delta wing of moderate sweep angle for pitch rates that extend over an eightfold range.

State 1 in Fig. 9 includes a positive bifurcation-line-like pattern $A$ originating from the apex, a saddle point $S$ located close to the intersection of leading and trailing edges, and a negative bifurcation line $BL^-$ along the leading edge, having a length of approximately one-third of the length of the leading edge.

State 2 involves the same positive bifurcation-line-like pattern $A$ near the plane of symmetry of the wing and a negative bifurcation line $BL^-$ along the leading edge, of smaller length relative to that of state 1. In addition, there are a number of small-scale foci of

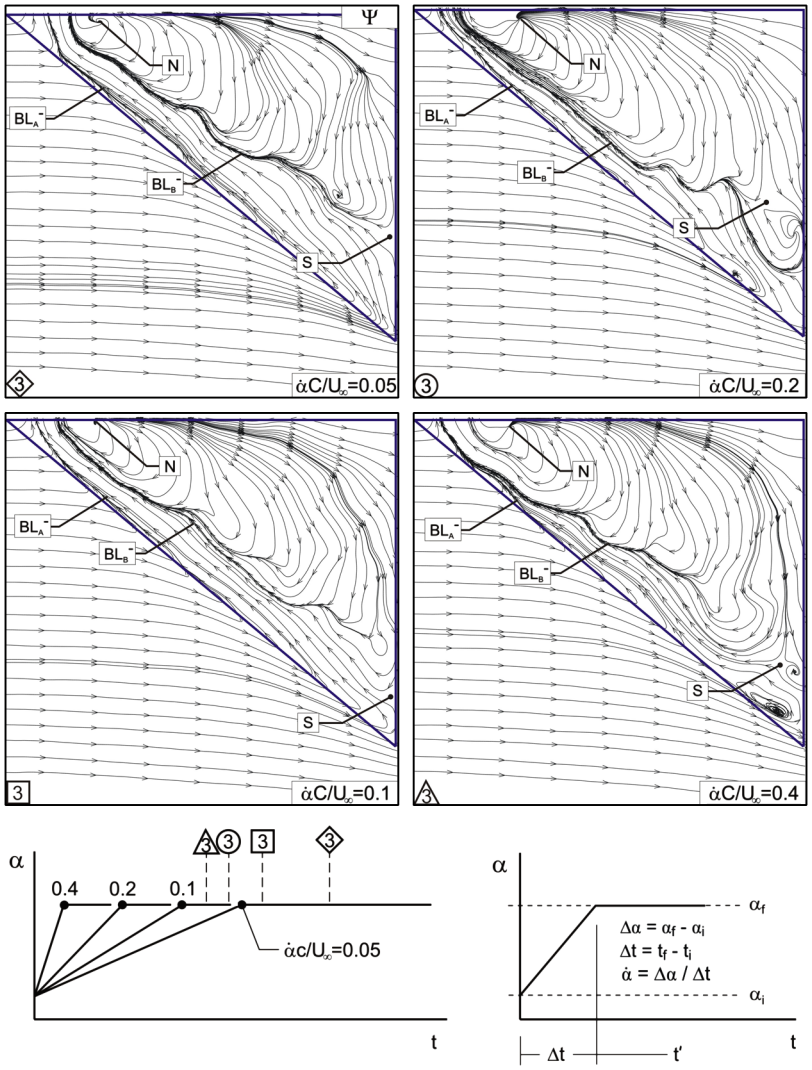


**Fig. 8 Patterns of instantaneous streamline topology Ψ at universal state 3 for different pitch rates $\dot{\alpha}C/U_\infty$.**

separation $F^-$ and two saddle points $S$ along the leading edge. These patterns of critical points represent the transition between the pattern of state 1 and a fundamentally different pattern of state 3.

In state 3, designated in Fig. 9, the positive bifurcation-line-like pattern $A$ is no longer visible. Instead, a well-defined node of attachment $N^+$ is present. A radical change compared to the previous states is that the negative bifurcation line $\mathrm{BL}^-$ is now oriented in the upstream direction toward the apex and its length has increased.

The patterns of critical points in state 4 represent the transition between the pattern of state 3 and a fundamentally different pattern of state 5. There are two small-scale negative bifurcation lines $\mathrm{BL}_A^-$ and $\mathrm{BL}_B^-$ close to the center and the apex of the wing, indicated with subscripts $A$ and $B$, respectively. The well-defined node of attachment $N^+$ of state 3 moves further toward the center of the wing, and it is no longer well-defined. The location of the saddle point $S$ moves closer to the intersection of leading and trailing edges.

State 5 is the final state. It occurs as an instant close to the completion of the relaxation process. This state closely resembles the steady state pattern, which includes a large-scale swirl pattern with a well-defined center, i.e., focus of separation $F^-$, located at approximately two-thirds of the chord. The location of the saddle point $S$, present in state 4, remains the same, and there is a very small negative bifurcation line $\mathrm{BL}^-$ close to the apex.

### B. Time Delays for Onset of Universal States

Although the same universal states occur in an ordered sequence for each pitch rate, the time delay from termination of the motion to their onset is expected to depend on the value of dimensionless pitch rate $\dot{\alpha}C/U_\infty$. Figure 10 shows the angle of attack as a function of time during and after the pitching maneuver for all pitch rates. The times of occurrence of the universal states at each value of pitch rate are indicated with a different color and a different symbol. For example, blue diamonds represent $\dot{\alpha}C/U_\infty = 0.05$, green squares represent $\dot{\alpha}C/U_\infty = 0.1$, orange circles represent $\dot{\alpha}C/U_\infty = 0.2$, and red triangles represent $\dot{\alpha}C/U_\infty = 0.4$. The time difference between two consecutive states is indicated as $(t_{i\to i+1})^{\dot{\alpha}C/U_\infty}$, where the subscript $i$ refers to the universal state number, and the superscript represents the pitch rate. For example, the time to go from state 2 to state 3 for the pitch rate of 0.2 is indicated as $(t_{2\to 3})^{0.2}$.

Five different universal states, as defined previously, can be observed for each pitch rate, except for state 5 at the maximum pitch rate of $\dot{\alpha}C/U_\infty = 0.4$, because of insufficient image-capturing time. These states involve the distinct patterns defined in Fig. 9.

For all values of pitch rate, at and after state 5, the flow is fully relaxed and the flow patterns have essentially converged to a steady state. For the minimum pitch rate of $\dot{\alpha}C/U_\infty = 0.05$, the flow distortion is minimal at the end of the maneuver, and state 1 is defined to be the pattern of near-surface topology that occurs at termination of the pitching maneuver. At successively larger values of pitch rate, the time elapsed between the termination of maneuver and the occurrence of the universal state 1 increases dramatically.

It is also apparent from Fig. 10 that the time delay between subsequent states is nearly independent of pitch rate. In other words, the time delay between universal state 1 and universal state 5, i.e., relaxation, is practically constant for all pitch rates.

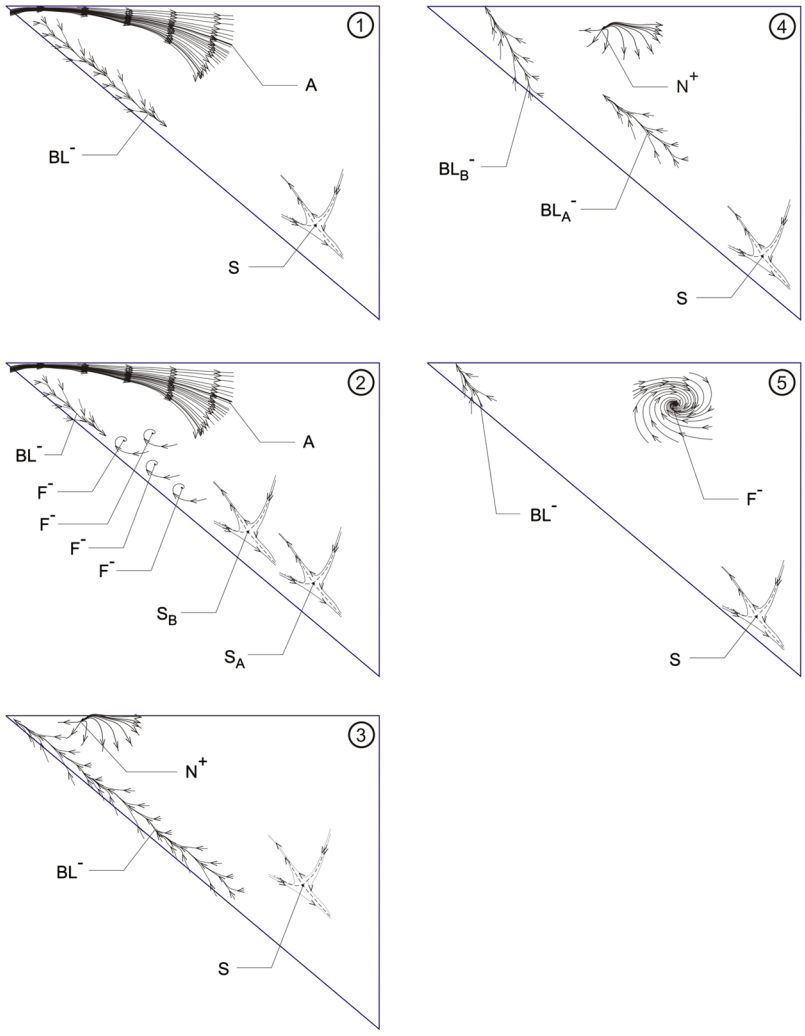


**Fig. 9 Definition of universal states during the relaxation process, in terms of critical points and topological features.**

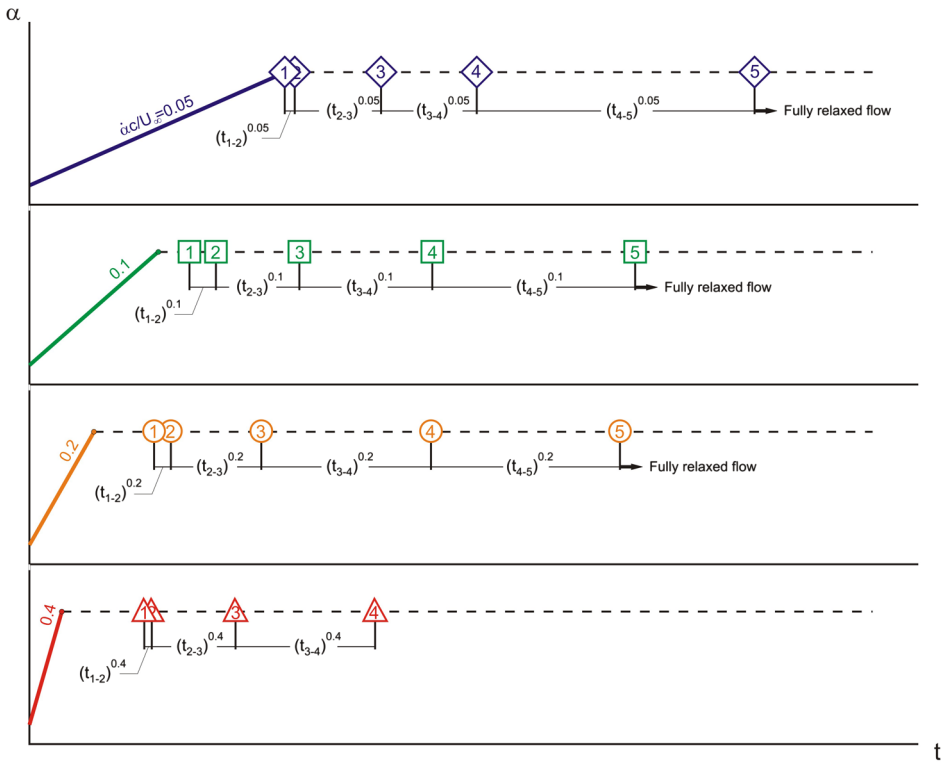


**Fig. 10 Times of occurrence of universal states during relaxation for different pitch rates $\dot{\alpha}C/U_\infty$.**

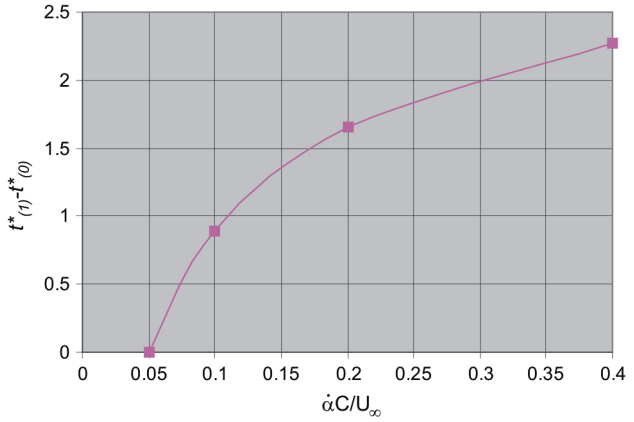


**Fig. 11 Time elapsed between termination of the pitch-up maneuver and the occurrence of universal state 1 as a function of pitch rate $\dot{\alpha}C/U_\infty$. Time $t^*$ is defined as $t'U_\infty/C$.**

The time elapsed between termination of the pitch-up maneuver and the occurrence of universal state 1 is given in Fig. 11 for all values of pitch rate. It is clear that the variation of elapsed time is not linear.

In universal state 5, three-dimensional separation and stall occur on the wing. The time elapsed between the termination of the pitching maneuver and occurrence of universal state 5 can be defined as the time delay for the occurrence of large-scale, three-dimensional separation, and thereby the onset of stall, $t_{stall}$. The value of $t_{stall}$ is the sum of the time between termination of the maneuver and the occurrence of universal state 1, and the time between the occurrence of universal states 1 and 5. As shown in Fig. 10, the time between the occurrence of universal states 1 and 5 is constant for all pitch rates. The time between termination of the maneuver and universal state 1, however, is not constant, but can be estimated for various pitch rates with the simple curve fit shown in Fig. 11. This approach is useful in predicting the time delay for the onset of stall, $t_{stall}$ for a wide range of pitch rate.

In conclusion, irrespective of the severity of the flow distortion at the end of the pitching maneuver, the relaxation of the flow involves the same sequence of universal states. The time delay to occurrence of the first universal state is very sensitive to the pitch rate. The delay between subsequent states is, however, nearly independent of pitch

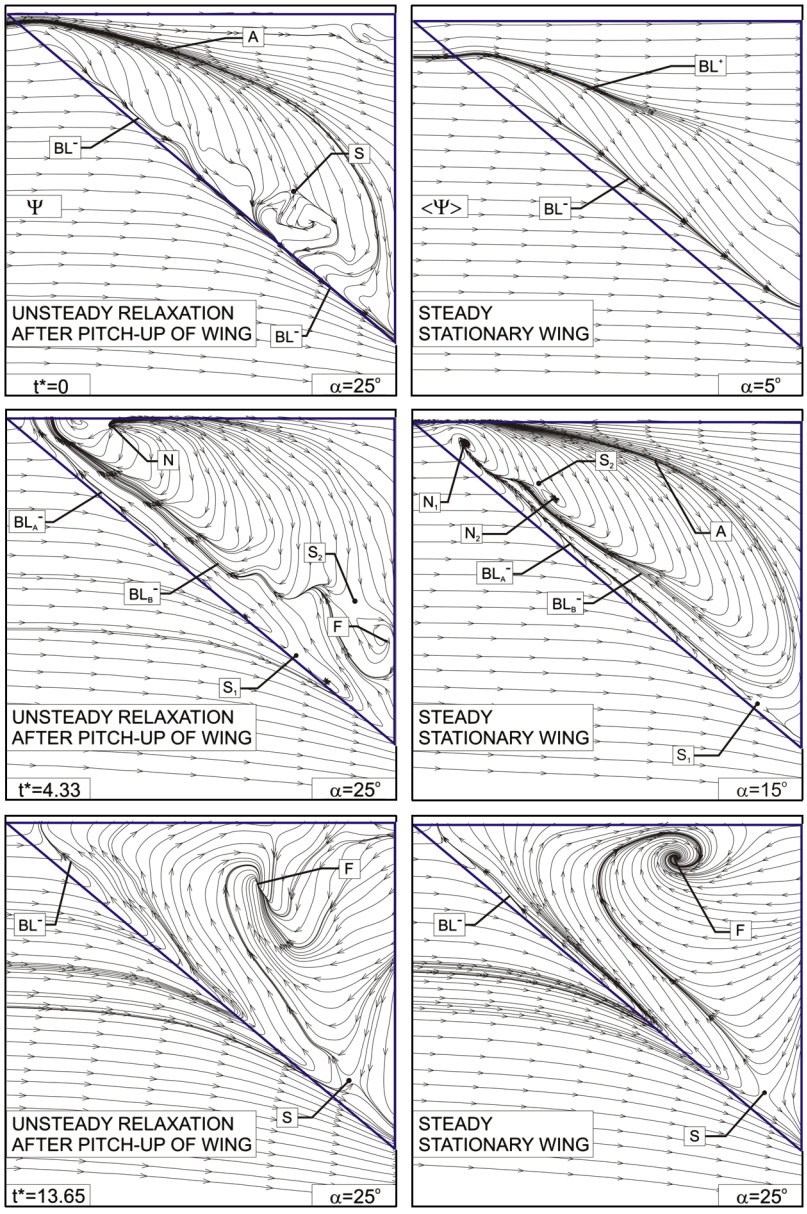


**Fig. 12 Comparison of instantaneous patterns of streamline topology $\Psi$ as a function of $t^*$ during the relaxation process for a pitch rate of $\dot{\alpha}C/U_\infty = 0.2$, and time-averaged patterns of streamline topology $\langle\Psi\rangle$ along a stationary wing at different values of angle of attack $\alpha$.**

rate. An approach is introduced for predicting the time delay from termination of the maneuver to onset of three-dimensional separation and stall on delta wings of moderate sweep angle.

## VI. Relation of Time-Averaged Topology to Instantaneous Topology

This section focuses on the analogies between the time-averaged patterns during the relaxation process following the pitch-up maneuver as well as the patterns in absence of a maneuver and the instantaneous patterns at termination of the pitching maneuver.

Su et al. [19] classified the types of separated flows above delta wings, in relation to the topology along the surface of the wings for a wide range of sweep angle $\Lambda$ and angle of attack $\alpha$. According to their schematic classification, as shown in Su et al. [19] (Fig. 4 on page 404), the time-averaged flow patterns on the surface of the stationary delta wing used in the present investigation, having $\Lambda = 50^\circ$ and $\alpha = 25^\circ$, fall into the general category of a spiral flow. That is, there is a spiral point (focus $F$ of separation) on each half of the wing, and unsteady shedding of vortices occurs from the foci $F$. In Su et al. [19], at $\alpha = 15^\circ$, the pattern of topology along the surface of the wing was undefined, and above the surface of the wing, bursting of the leading-edge vortex occurs. That is, a leading-edge vortex is present and its breakdown location is between the apex and the trailing edge. The flow patterns above the wing at $\alpha = 5^\circ$ had the form of a bubble vortex. According to Su et al. [19], in this case, the free shear layer has rolled up but no concentrated vortex core is formed, and the corresponding pattern of topology along the surface of the wing was undefined.

Figure 12 shows, in the left column, instantaneous patterns of streamline topology as a function of normalized time $t^*$ during relaxation for a pitch rate of $\dot{\alpha}C/U_\infty = 0.2$ and, in the right column, time-averaged patterns of streamline topology along a stationary wing at different values of angle of attack.

A direct comparison of the images corresponding to the maneuvering wing with images of the stationary wing indicates similarities in the streamline topology between two cases, in which they exhibit common topological features and critical points. For example, the streamline topology of the stationary wing at $\alpha = 5^\circ$ is very similar to that of the maneuvering wing at $t^* = 0$. They both show a pair of negative and positive bifurcation lines: $\mathrm{BL}_A^-$ and $\mathrm{BL}_B^-$ along the stationary-wing image at $\alpha = 5^\circ$ and $\mathrm{BL}^-$ and $A$ (positive bifurcation-line-like pattern) for the maneuvering wing at $t^* = 0$. Likewise, the aforementioned patterns for the stationary wing at $\alpha = 15^\circ$ are very similar to those for the maneuvering wing at $t^* = 4.33$. Their common topological features are a well-defined node of attachment close to apex: $N_1$ in the stationary wing at $\alpha = 15^\circ$, and $N$ for the maneuvering wing at $t^* = 4.33$, a saddle point $S_1$ close to the intersection of leading and trailing edges, and two negative bifurcation lines $\mathrm{BL}_A^-$ and $\mathrm{BL}_B^-$. The aforementioned patterns for the stationary wing at $\alpha = 25^\circ$ are very similar to those for the maneuvering wing at $t^* = 13.65$. They both include a focus $F$ of separation, a negative bifurcation line $\mathrm{BL}^-$ along the leading edge close to apex, and a saddle point $S$ close to the intersection of leading and trailing edges.

In summary, the foregoing comparisons demonstrate that the near-surface topological patterns observed during the early stages of the relaxation process (following termination of a maneuver) are similar in form to the near-surface patterns on the corresponding stationary wing at smaller angles of attack. This similarity of patterns is due to the time lag of the flow structure following cessation of the wing maneuver.

## VII. Conclusions

The time evolution of the near-surface flow patterns is characterized along a delta wing of moderate sweep angle using a technique of high-image-density single camera particle image velocimetry. Emphasis is on the patterns following completion of a linear ramplike pitching motion for a wide range of pitch rate. Patterns of velocity vectors and streamline topology, including critical points and topological features allow definition of the effect of pitch rate. Dye visualization provided complementary insight. Similar investigations were performed for the flow patterns on a stationary delta wing as a function of static variation of angle of attack. The principal findings are as follows:

1) Five different universal states of the near-surface topology can be defined during the relaxation process that follows termination of the pitching motion. Such states can be identified over an eightfold range of pitch rate. These states involve distinct patterns that can be defined in terms of topological features and define the time evolution of flow structure on a delta wing of moderate sweep angle.

2) The near-surface patterns at the instant corresponding to termination of the maneuver are a strong function of the magnitude of pitch rate and show substantial variation. Remarkably, despite the large differences in the state of the flow at the beginning of the relaxation process, the near-surface patterns evolve in the aforementioned sequence of universal states. That is, irrespective of the severity of the flow distortion at the end of the pitching maneuver, the relaxation of the flow involves the same sequence of universal states.

3) During evolution of flow following termination of the pitching maneuver, it is demonstrated that the time delay to occurrence of the first state is very sensitive to the magnitude of the pitch rate. The delay between subsequent states is, however, nearly independent of pitch rate. The time delay to occurrence of the first universal state is not constant, but can be estimated for variations of pitch rate with a simple curve fit. The time delay between the occurrence of the first universal state and of the fifth universal state is, however, nearly constant for all pitch rates. Therefore, a stall time can be defined as the sum of: the time between termination of maneuver and occurrence of the first universal state, which is a function of pitch rate, and the time between the occurrence of the first universal state and occurrence of the fifth universal state, which is independent of pitch rate. This approach provides an indication of the onset of three-dimensional separation and stall along the surface of the wing for a wide range of pitch rate.

4) The universal states are defined in terms of near-surface topology using critical points. This approach allows identification of regions of separation and reattachment, as well as centers of large-scale and small-scale recirculation zones along the surface of the wing. During the relaxation process, these critical points undergo alterations, or, in some cases, transformation to another type of critical point. This time evolution of the patterns of critical points is complemented by dye visualization of the flow pattern along the wing, which defines the evolution of the leading-edge vortex and the onset of separation and stall. Furthermore, it is demonstrated that there exists a critical universal state, which marks an abrupt transformation between two distinctly different states of the near-surface pattern of critical points.

5) Time-averaged patterns of the near-surface topology were evaluated at various values of angle of attack of the corresponding stationary wing. It is demonstrated that the sequence of the topological patterns observed during the early stages of the relaxation process is similar to the patterns on the stationary wing at successively smaller angles of attack.

## References

[1] Gursul, I., Gordnier, R., and Visbal, M., "Unsteady Aerodynamics of Nonslender Delta Wings," *Progress in Aerospace Sciences*, Vol. 41, No. 7, Oct. 2005, pp. 515–557. doi:10.1016/j.paerosci.2005.09.002

[2] Gursul, I., "Recent Developments in Delta Wing Aerodynamics," *The Aeronautical Journal*, Vol. 108, No. 1087, Sept. 2004, pp. 437–452.

[3] Ol, M. V., and Gharib, M., "Leading-Edge Vortex Structure of Nonslender Delta Wings at Low Reynolds Number," *AIAA Journal*, Vol. 41, No. 1, 2003, pp. 16–26. doi:10.2514/2.1930

[4] Gursul, I., Taylor, G., and Wooding, C. L., "Vortex Flows over Fixed-Wing Micro Air Vehicles," AIAA Paper 2002-0698, 2002.

[5] Taylor, G. S., Schnorbus, T., and Gursul, I., "An Investigation of Vortex Flows over Low Sweep Delta Wings," AIAA Fluid Dynamics Conference, AIAA Paper 2003-4021, Orlando, FL, 23–26 June 2003.

[6] Miau, J. J., Kuo, K. T., Liu, W. H., Hsieh, S. J., Chou, J. H., and Lin, C. K., "Flow Developments Above 50-Deg Sweep Delta Wings with Different Leading-Edge Profiles," *Journal of Aircraft*, Vol. 32, No. 4, 1995, pp. 787–794. doi:10.2514/3.46792

[7] Gordnier, R. E., and Visbal, M. R., "Higher-Order Compact Difference Scheme Applied to the Simulation of a Low Sweep Delta Wing Flow," 41st AIAA Aerospace Sciences Meeting and Exhibit, AIAA Paper 2003-0620, Reno, NV, Jan. 2003.

[8] Yaniktepe, B., and Rockwell, D., "Flow Structure on a Delta Wing of Low Sweep Angle," *AIAA Journal*, Vol. 42, No. 3, March 2004, pp. 513–523. doi:10.2514/1.1207

[9] Yavuz, M. M., "Origin and Control of the Flow Structure and Topology on Delta Wings," Ph.D. Dissertation, Lehigh Univ., Bethlehem, PA, 2006.

[10] Legendre, R., "Lignes de Courent d'un Ēcoulement Continu," *La Recherche Aérospatiale*, No. 105, 1965, pp. 3–9.

[11] Hunt, J. C. R., Abell, C. J., Peterka, J. A., and Woo, H., "Kinematical Studies of the Flows Around Free or Surface-Mounted Obstacles: Applying Topology to Flow Visualization," *Journal of Fluid Mechanics*, Vol. 86, Pt. 1, 1978, pp. 179–200. doi:10.1017/S0022112078001068

[12] Tobak, M., and Peake, D. J., "Topology of Three-Dimensional Separated Flows," *Annual Review of Fluid Mechanics*, Vol. 14, 1982, pp. 61–85. doi:10.1146/annurev.fl.14.010182.000425

[13] Moffatt, H. K., and Tsinober, A., "Topological Fluid Mechanics," *Proceedings of the IUTAM Symposium*, Cambridge Univ. Press, New York, 1990, pp. 372–408.

[14] Peake, D. J., and Tobak, M., "Three-Dimensional Separation and Reattachment," *High Angle-of-Attack Aerodynamics*, AGARD, Lecture No. 121, Neuilly-sur-Seine, France, 1982, pp. 1-1–1-14.

[15] Peake, D. J., and Tobak, M., "Three-Dimensional Flows About Simple Components at Angle-of-Attack," *High Angle-of-Attack Aerodynamics*, AGARD, Lecture No. 121, Neuilly-sur-Seine, France, 1982, pp. 1-1–1-56.

[16] Perry, A. E., and Hornung, H. G., "Some Aspects of Three-Dimensional Separation. Part II. Vortex Skeletons," *Zeitschrift für Flugwissenschaften und Weltraumforschung*, Vol. 8, 1984, pp. 155–160.

[17] Perry, A. E., and Chong, M. S., "A Description of Eddying Motions and Flow Patterns Using Critical-Point Concepts," *Annual Review of Fluid Mechanics*, Vol. 19, 1987, pp. 125–155. doi:10.1146/annurev.fl.19.010187.001013

[18] Dallman, U., and Schulte-Werning, B., "Topological Changes of Axisymmetric and Non-Axisymmetric Vortex Flows," *Proceedings of the IUTAM Symposium*, Cambridge Univ. Press, New York, 1990, pp. 372–383.

[19] Su, W., Liu, M., and Liu, Z., "Topological Structures of Separated Flows About a Series of Sharp-Edged Delta Wings at Angles of Attack up to 90°," *Topological Fluid Mechanics*, edited by H. K. Moffatt, and A. Tsinober, Cambridge Univ. Press, New York, 1990.

[20] Lazos, B., "Surface Topology on the Wheels of a Generic Four-Wheel Landing Gear," *AIAA Journal*, Vol. 40, No. 12, Dec. 2002, pp. 2402–2412. doi:10.2514/2.1608

[21] Taylor, G. S., and Gursul, I., "Unsteady Vortex Flows and Buffeting of a Low Sweep Delta Wing," 42nd AIAA Aerospace Sciences Meeting and Exhibit, AIAA Paper 2004-1066, Reno, NV, Jan. 2004.

[22] Rockwell, D., "Three-Dimensional Flow Structure on Delta Wings at High Angle-of-Attack: Experimental Concepts Issues," AIAA Paper 93-0550, Jan. 1993.

[23] Visbal, M. R., "Computational and Physical Aspects of Vortex Breakdown on Delta Wings," AIAA Paper 95-0585, Jan. 1995.

[24] Maltby, R. L., Engler, P. B., and Keating, R. F. A., "Some Exploratory Measurements of Leading-Edge Vortex Positions on a Delta Wing Oscillating in Heave," Aeronautical Research Council, Research and Memorandum No. 3410, London, July 1963.

[25] Gursul, I., "Review of Unsteady Vortex Flows over Slender Delta Wings," *Journal of Aircraft*, Vol. 42, No. 2, March–April 2005, pp. 299–319. doi:10.2514/1.5269

[26] Lambourne, N. C., Bryer, D. W., and Maybrey, J. F. M., "The Behaviour of the Leading-Edge Vortices over a Delta Wing Following a Sudden Change of Incidence," Aeronautical Research Council, Research and Memorandum No. 3645, London, March 1969.

[27] Gad-el-Hak, M., and Ho, C. M., "Pitching Delta Wing," *AIAA Journal*, Vol. 23, No. 11, 1985, pp. 1660–1665. doi:10.2514/3.9147

[28] Gursul, I., and Yang, H., "On Fluctuations of Vortex Breakdown Location," *Physics of Fluids*, Vol. 7, No. 1, 1995, pp. 229–231. doi:10.1063/1.868724

[29] Gursul, I., and Ho, C. M., "Vortex Breakdown over Delta Wings in Unsteady Freestream," *AIAA Journal*, Vol. 32, No. 2, Feb. 1994, pp. 433–436. doi:10.2514/3.12003

[30] Miau, J. J., Chang, R. C., Chou, J. H., and Lin, C. K., "Nonuniform Motion of Leading-Edge Vortex Breakdown on Ramp Pitching Delta Wings," *AIAA Journal*, Vol. 30, No. 7, July 1992, pp. 1691–1702. doi:10.2514/3.11125

[31] Visbal, M. R., and Gordnier, R. E., "Pitch Rate and Pitch-Axis Location Effects on Vortex Breakdown Onset," *Journal of Aircraft*, Vol. 32, No. 5, 1995, pp. 929–935. doi:10.2514/3.46820

[32] Reynolds, G. A., and Abtahi, A. A., "Instabilities in Leading-Edge Vortex Development," AIAA Paper 87-2424, 1987.

[33] Magness, C., Robinson, O., and Rockwell, D., "Control of Leading-Edge Vortices on a Delta Wing," AIAA Paper 89-0999, 1989.

[34] Jarrah, M. A. M., "Visualization of the Flow about a Delta Wing Maneuvering in Pitch to Very High Angle of Attack," *International Symposium on Nonsteady Fluid Dynamics*, edited by J. A. Miller, and D. P. Telionis, American Society of Mechanical Engineers, Fluids Engineering Div., New York, 1990, pp. 109–117.

[35] Atta, R., and Rockwell, D., "Hysteresis of Vortex Development and Breakdown on an Oscillating Delta Wing,"*AIAA Journal*, Vol. 25, No. 11, 1987, pp. 1512–1513. doi:10.2514/3.9812

[36] LeMay, S. P., Batill, S. M., and Nelson, R. C., "Vortex Dynamics on a Pitching Delta Wing," *Journal of Aircraft*, Vol. 27, No. 2, 1990, pp. 131–138. doi:10.2514/3.45908

[37] Woffelt, K. W., "Investigation of the Movement of Vortex Burst Position with Dynamically Changing Angle of Attack for Schematic Delta Wing in a Water Tunnel with Correlation to Similar Studies in Wind Tunnels," *Aerodynamic and Related Hydrodynamic Studies Using Water Facilities*, AGARD CP-413, Neuilly-sur-Seine, France, 1986.

[38] Lin, J. C., and Rockwell, D., "Transient Structure of Vortex Breakdown on a Delta Wing," *AIAA Journal*, Vol. 33, No. 1, Jan. 1995, pp. 6–12. doi:10.2514/3.12325

[39] Magness, C., Robinson, O., and Rockwell, D., "Instantaneous Topology of the Unsteady Leading Edge Vortex at High Angle of Attack," *AIAA Journal*, Vol. 31, No. 8, Aug. 1993, pp. 1384–1391. doi:10.2514/3.11786

[40] Yavuz, M. M., Elkhoury, M., and Rockwell, D., "Near-Surface Topology and Flow Structure on a Delta Wing," *AIAA Journal*, Vol. 42, No. 2, 2004, pp. 332–340. doi:10.2514/1.3499

[41] Goruney, T., "Investigation of Flow Structure on a Stationary and Pitching Delta Wing of Moderate Sweep Angle Using Stereoscopic Particle Image Velocimetry," Ph.D. Dissertation, Lehigh Univ., Bethlehem, PA, 2008.

[42] Lamar, J. E., "In-Flight and Wind Tunnel Leading-Edge Vortex Study on the F-106B Airplane," NASA Langley Research Center, Hampton, VA, 1986.

[43] Riley, A. J., and Lowson, M. V., "Development of a Three-Dimensional Free Shear Layer," *Journal of Fluid Mechanics*, Vol. 369, 1998, pp. 49–89.

F. Coton
*Associate Editor*